Simulation of Water Age and Residence Time in New York Bight

WEIFENG G. ZHANG, JOHN L. WILKIN, AND OSCAR M. E. SCHOFIELD

Institute of Marine and Coastal Sciences, Rutgers, The State University of New Jersey, New Brunswick, New Jersey

ABSTRACT

The time scales on which river inflows disperse in the coastal ocean are relevant to a host of biogeochemical and environmental processes. These time scales are examined in a modeling study of the Hudson River plume on its entry to the New York Bight (NYB). Constituent-oriented age and residence-time theory is applied to compute two time scales: mean age, which is calculated from the ratio of two model tracers, and residence time, which is calculated using the adjoint of the tracer conservation equation.

Spatial and temporal variability associated with river discharge and wind is investigated. High river discharge lowers surface water age and shortens residence time in the apex of the NYB. Easterly winds increase surface water age and extend the duration waters along the Long Island coast remain in the NYB apex. Southerly winds increase age along the New Jersey coast but drive a decrease in age of offshore surface waters and prolong the time that surface waters close to the New Jersey coast stay in the NYB apex. Residence time along the Long Island coast is high in spring and summer because of the retention of water north of the Hudson shelf valley.

Patterns of modeled surface water age and an age proxy computed from the ratio of satellite-measured irradiance in two channels show qualitative agreement. A least squares fit gives a statistically significant empirical relationship between the band ratio and modeled mean age for NYB waters.

1. Introduction

Time-scale analysis (water age and residence time) has utility for estimating ventilation rates of lakes, estuaries, and ocean basins (England 1995; Hohmann et al. 1998; Jenkins 1987); inferring ocean circulation and mixing (Fine 1995; Haine et al. 1998; Schlosser et al. 2001; Wunsch 2002); and studying rates of biogeochemical processes (Hohmann et al. 1998; Sarmiento et al. 1990; Weiss et al. 1991). Water age is not directly observable, so transient tracers, isotopes, and anthropogenic tracers are used to infer age, by which it is generally meant the elapsed time since the water was last in contact with the tracer source. Most tracer age derivations assume negligible mixing and diffusion (Fine 1995; Hohmann et al. 1998; Jenkins 1987; Schlosser et al. 2001; Weiss et al. 1991), although these processes can substantially divert tracer-based age from real age (Deleersnijder et al. 2001; Delhez et al. 2003; Thiele and Sarmiento 1990; Waugh et al. 2003). In numerical modeling, a common approach is to release

many tracers and extract time-scale information from their differential transport (Gao et al. 2005; Monsen et al. 2002). This method requires substantial computation if spatial and temporal detail is sought. Methods for directly simulating these time scales were introduced by Jenkins (1987) and Sarmiento et al. (1990), who derived tracer-based age conservation equations. The concept of an ideal age tracer followed and has been compared with radiotracer age in idealized simulations (Thiele and Sarmiento 1990), and it has been used to simulate global ocean ventilation rates in a general circulation model (England 1995).

Further developments in modeling time scales have followed two approaches: constituent-oriented age and residence-time theory (CART; Deleersnijder et al. 2001; Delhez 2006; Delhez et al. 2004, 2006, 1999) and Green's function-based transit time distribution theory (TTD; Haine and Hall 2002; Hall and Plumb 1994; Holzer and Hall 2000). Both approaches can provide the same information but have different priorities. TTD was developed in the context of steady flow and emphasizes computing the transit time spectrum. This gives an age spectrum when expressed as a probability density function (PDF) of transit times since a tracer last had contact with its

Corresponding author address: Weifeng G. Zhang, Woods Hole Oceanographic Institution, MS 9, Woods Hole, MA 02543.
E-mail: wzhang@whoi.edu

origin and a residence-time spectrum when the PDF is of transit time from a certain point to first contact with a location where it can exit a defined domain. For time-varying flows, the computation of the full age and residence-time spectrum becomes prohibitive, especially for highly resolved coastal ocean applications, even when exploiting the recently described transport matrix framework (Khatiwala 2007) to accelerate simulations. CART provides a cheap way to compute the mean of the spectrum (i.e., "mean tracer age"), which is defined as the mass-weighted, arithmetic average of the time elapsed since the tracer left the source region, and the "mean residence time," which is defined as the mass-weighted, arithmetic average of the time needed for the tracer to leave a domain of interest. Neither mean age nor mean residence-time fully characterize the water mass movement (Hall and Haine 2002). Nevertheless, this information is still very useful for studying spatial patterns of circulation and mixing and their associated time scales, which is the main objective here and is instructive when considering many coastal ocean biogeochemical processes.

Focusing on time scales associated with the spreading of river source waters across the inner shelf, this paper applies CART to the circulation of the Hudson River discharge in the New York Bight (NYB). The NYB is adjacent to a wide, shallow continental shelf; on this coast, wind, large-scale shelf-wide circulation, and variable bathymetry all play roles in driving local circulation and dispersing the Hudson River plume (Castelao et al. 2008; Chant et al. 2008; Garvine 2004; Johnson et al. 2003; Wong 1999; Yankovsky et al. 2000; Zhang et al. 2009a), which is a major source of suspended matter, nutrients, dissolved organic matter, and contaminants to the NYB (Adams et al. 1998; Howarth et al. 2006; Schofield et al. 2009, submitted to *J. Geophys. Res.*, hereafter SCH). Transport of these materials from the estuary to the shelf regulates local biogeochemical processes (Geyer et al. 2001; Moline et al. 2008; SCH) for which time scales are key factors (Howarth et al. 2006; Malone and Chervin 1979).

The path of the Hudson River plume is highly mobile, largely controlled by local wind, and influenced by bottom topography (Chant et al. 2008; Choi and Wilkin 2007; Zhang et al. 2009a). Under high discharge conditions, the plume often forms a low salinity "bulge" at the NYB apex area extending 30–40 km from the coast. The bulge recirculates water and potentially traps tracers there, causing less than ½ of the total freshwater outflow to enter the southward current along the coast of New Jersey. The freshwater outflow pathways vary with season (Zhang et al. 2009a). In summer, when upwelling favorable winds prevail, the recirculation bulge is weak and the river plume tends to move directly offshore. During the rest of the year, winds have a significant offshore component and the recirculation bulge is more prevalent, ultimately feeding a strong coastal current along the New Jersey coast and weaker current along the Long Island coast. The effect of these pathways on the time scale of freshwater dispersal onto and out of the NYB apex is the focus of this paper.

The CART theory is summarized in section 2. Section 3 introduces the regional model configuration and verification. Results of the mean age simulations are presented in section 4, and those for mean residence time are presented in section 5. Section 6 summarizes the results and their relevance to regional ocean circulation.

2. CART

Following Delhez et al. (1999), Deleersnijder et al. (2001), Delhez et al. (2004), Delhez (2006), and Delhez and Deleersnijder (2006), derivations of mean age and residence time are summarized here.

a. Mean age

Suppose a water parcel located at $\mathbf{x}$ at time t contains dissolved tracer having an age spectrum concentration distribution $c(t, \mathbf{x}, \tau)$, where τ is the age (i.e., the time since the tracer was released into the water). The equation for age spectrum concentration is

$$\frac{\partial c}{\partial t} = p - d - \mathbf{\nabla} \cdot (\mathbf{u}c - \mathbf{K} \cdot \mathbf{\nabla}c) - \frac{\partial c}{\partial \tau}, \qquad (1)$$

where p and d are the rates of production and destruction, respectively (in this application, these terms are zero, with production effectively entering only in the river source boundary condition); $\mathbf{u}$ is the flow velocity; and $\mathbf{K}$ is the eddy diffusivity tensor. The last term on the right-hand side expresses the aging of the tracer. Equation (1) can be used to simulate the age spectrum concentration directly, but at considerable computational cost if hundreds of tracers are activated to resolve the age spectrum well.

The concentration of tracer in the fluid is the integral of the age spectrum with respect to age, $C(t, \mathbf{x}) = \int_0^\infty c(t, \mathbf{x}, \tau)\, d\tau$, whereas the mean age $a(t, \mathbf{x})$ is the first moment of the age spectrum, $a(t, \mathbf{x}) = \int_0^\infty \tau c(t, \mathbf{x}, \tau)\, d\tau / C(t, \mathbf{x})$. If we define an age concentration tracer, $\alpha(t, \mathbf{x}) = \int_0^\infty \tau c(t, \mathbf{x}, \tau)\, d\tau$, then

$$a(t, \mathbf{x}) = \frac{\alpha(t, \mathbf{x})}{C(t, \mathbf{x})}. \qquad (2)$$

The $\lim_{\tau \to \infty} c(t, \mathbf{x}, \tau) = 0$, so integrating (1) over τ gives the time rate of change of the total concentration of the tracer,

$$\frac{\partial C}{\partial t} = P - D - \nabla \cdot (\mathbf{u}C - \mathbf{K} \cdot \nabla C). \tag{3}$$

Here, $P(t, \mathbf{x}) = c(t, \mathbf{x}, \tau = 0) + \int_0^\infty p(t, \mathbf{x}, \tau) \, d\tau$ is the source of tracer and $D(t, \mathbf{x}) = \int_0^\infty d(t, \mathbf{x}, \tau) \, d\tau$ is the sink. Equation (3) is the conservation equation solved in numerical circulation models. Multiplying (1) by τ, then integrating over τ and applying a reasonable assumption, $\lim_{\tau \to \infty} c(t, \mathbf{x}, \tau) = 0$, we obtain the age concentration equation,

$$\frac{\partial \alpha}{\partial t} = C + \pi - \lambda - \nabla \cdot (\mathbf{u}\alpha - \mathbf{K} \cdot \nabla \alpha), \tag{4}$$

where $\pi(t, \mathbf{x}) = \int_0^\infty \tau p(t, \mathbf{x}, \tau) \, d\tau$ and $\lambda(t, \mathbf{x}) = \int_0^\infty \tau d(t, \mathbf{x}, \tau) \, d\tau$. The age concentration is coupled with (3) through the first term on the right-hand side; if tracer is present in the fluid, then $C > 0$ and the age concentration grows in time proportionately.

The ideal water age equation of Thiele and Sarmiento (1990) and England (1995) is

$$\frac{\partial a}{\partial t} = 1 - \nabla \cdot (\mathbf{u}a - \mathbf{K} \cdot \nabla a). \tag{5}$$

This describes the age of the water itself, as opposed to the age of the tracer, and can be derived from (4) in the case that $C = 1$ everywhere and there are no sources and sinks of a in the domain interior.

Equations (3) and (4) can be solved numerically using an ocean model. We set initial conditions for both C and α of zero and release tracer after the initial time from a source at the head of the modeled Hudson River. We are therefore asking the following question: How long has it been since the Hudson River sourced water at an offshore location $\mathbf{x}$ and time t first entered the ocean? Equation (2) gives this mean age of river source water everywhere. Where the newly released tracer has not yet reached, C is zero and the mean age is undefined. This method is easily implemented in most Eulerian numerical models because it requires only two tracers and the addition of the first term on the right-hand side of (4).

b. Residence time

We define residence time θ as the time taken by tracer to leave a control domain ω. Consider a volume of tracer located at $\mathbf{x}_0$ (inside the control domain) at time $t = t_0$ with volume V_0 and concentration $C(t_0, \mathbf{x}_0)$ (volume percentage), $C(t_0, \mathbf{x}) = C_0 \delta(\mathbf{x}_0)$, where δ is the Dirac delta function. The tracer leaves the control domain ω gradually. The volume of the tracer remaining in the control domain at time t is an integration of the tracer concentration over the whole control domain,

$$V(t) = \int_\omega C(t, \mathbf{x}) \, d\omega = \int_{\omega_T} C(t, \mathbf{x}) f(\mathbf{x}) \, d\omega, \tag{6}$$

where ω_T is the volume of the total model domain that is larger than or equal to ω and f is a function that delineates the control domain,

$$f(\mathbf{x}) = \delta_\omega = \begin{cases} 1 & \mathbf{x} \in \omega \\ 0 & \mathbf{x} \notin \omega \end{cases}.$$

Here, we define a new variable δ_ω for concise notation in later equations.

Some fraction of the tracer leaves the control domain at time t_f having residence time $\theta = t_f - t_0$. The mean residence time of the tracer body in the control domain is

$$\overline{\theta}(t_0, \mathbf{x}_0) = \frac{1}{V_0} \int_{V_0} (t_f - t_0) \, dV. \tag{7}$$

Applying integration by parts and assuming that all of the tracer is flushed out of the control domain eventually [i.e., $V(t_f) = 0$ as $t_f \to \infty$], we can express the mean residence time as

$$\overline{\theta}(t_0, \mathbf{x}_0) = \frac{1}{V_0} \int_{t_0}^\infty V(t_f) \, dt_f. \tag{8}$$

These equations show how point injections of tracer in a model can be used to obtain the residence time. However, one injection only gives the residence time at one place at one time, and to resolve spatial and temporal variability requires many injections and simulations, at substantial computational cost. This problem can be circumvented.

We write (6) in inner-product form,

$$V(t_f) = \langle C(t_f, \mathbf{x}), f(\mathbf{x}) \rangle_{\omega_T}, \tag{9}$$

and note that (3) can be written, with P and D set to 0, in propagator form (Moore et al. 2004) $C(t_f, \mathbf{x}) = \mathbf{R}(t_0, t_f) C(t_0, \mathbf{x})$ because it is linear in the concentration C. Here, $\mathbf{R}(t_0, t_f)$ is the propagator matrix that advances the ocean state from time t_0 to t_f. Applying the Green's identity of the adjoint operator (Lanczos 1961) to (9), we obtain

$$\begin{aligned} V(t_f) &= \langle \mathbf{R}(t_0, t_f) C(t_0, \mathbf{x}), f(\mathbf{x}) \rangle_{\omega_T} \\ &= \langle C(t_0, \mathbf{x}), \mathbf{R}^\dagger(t_f, t_0) f(\mathbf{x}) \rangle_{\omega_T} = V_0 C^\dagger(t_0, \mathbf{x}_0). \end{aligned} \tag{10}$$

Here, $\mathbf{R}^\dagger(t_f, t_0)$ is the adjoint operator of (3) that propagates information backward from t_f to t_0 and

$C^{\dagger}(t_0, \mathbf{x}) = \mathbf{R}^{\dagger}(t_f, t_0)f(\mathbf{x})$ is the adjoint state tracer variable. The corresponding adjoint equation is

$$-\frac{\partial C^{\dagger}}{\partial t_0} = \nabla \cdot (\mathbf{u}C^{\dagger} + \mathbf{K} \cdot \nabla C^{\dagger}), \qquad (11)$$

which is integrated backward in time with initial conditions at t_f of $C^{\dagger}(t_f, \mathbf{x}) = f(\mathbf{x}) = \delta_{\omega}$. Equation (10) shows that $C^{\dagger}(t_0, \mathbf{x}_0)$ is the fraction of tracer that was initially located at $\mathbf{x}_0$ at time t_0 that remains in the control domain at time t_f; that is,

$$C^{\dagger}(t_0, \mathbf{x}_0) = \frac{V(t_f)}{V_0}.$$

From (8), we have

$$\bar{\theta}(t_0, \mathbf{x}_0) = \int_{t_0}^{\infty} C^{\dagger}(t_0, \mathbf{x}_0)\, dt_f. \qquad (12)$$

The ocean state is unsteady, so the fraction of tracer remaining differs for different time windows (t_0, t_f), even with same window duration; that is, $C^{\dagger}$ is a function of both t_0 and t_f [i.e., $C^{\dagger} = C^{\dagger}(t_0, t_f, \mathbf{x})$].

Let us now define a time T_f far in the future (i.e., $T_f \gg t_0$), when all tracer has been flushed out of the control domain; that is,

$$C^{\dagger}(t_0, T_f, \mathbf{x}) = 0. \qquad (13)$$

Integrating (11) over t_f from t_0 to T_f, applying Leibniz integral rule and using (12), we obtain the equation for the mean residence time:

$$-\frac{\partial \bar{\theta}}{\partial t_0} = \delta_{\omega} + \nabla \cdot (\mathbf{u}\bar{\theta} + \mathbf{K} \cdot \nabla \bar{\theta}), \qquad (14)$$

where $\bar{\theta} = \bar{\theta}(t_0, \mathbf{x})$. Integration of (14), backward in time, gives the mean residence time everywhere in the control domain for any time within the simulation window. However, the initial condition $\bar{\theta}(T_f, \mathbf{x})$ is unknown. Delhez et al. (2004) derived (14) and proposed initializing the mean age with $\bar{\theta}(T_f, \mathbf{x}) = 0$ and integrating sufficiently long that the influence of the initial condition vanishes; the required time can be determined from the solution to (11). The argument goes as follows: The initial condition of (11) is $C^{\dagger}(t_f, t_f, \mathbf{x}) = \delta_{\omega}$; because of the lack of forcing, $C^{\dagger}(t_0, t_f, \mathbf{x})$ gradually disperses away as the backward integration proceeds until $C^{\dagger}(t_0, t_f, \mathbf{x})$ approaches 0 and the effect of the initial condition vanishes. By virtue of the similarity of (11) and (14), we expect the effect of initial conditions to decay similarly in both equations. Therefore, we integrate (11) and (14)

simultaneously and the solution to (14) becomes valid when the solution to (11) approaches zero. Delhez (2006) proved the validity of this approach.

If the model domain is larger than the control domain ($\omega \subset \omega_T$), there are two ways to treat the area beyond the control domain (Delhez 2006; Delhez and Deleersnijder 2006). The first is to force the adjoint model state $\bar{\theta}(t_0, \mathbf{x})$ to be zero everywhere beyond the control domain. This is termed the "strict mean residence time" (Delhez et al. 2004). In the analysis of Lagrangian drifters, this is equivalent to ceasing to track a drifter the first time it crosses the control domain boundary. The second way is to let the adjoint solution evolve freely outside the control domain (Delhez 2006). This approach essentially gives the accumulated time spent by tracer in the control domain, which is called the "exposure time" (Monsen et al. 2002). In tracking drifters, this allows for reentry into the control domain.

3. Model configuration and verification

We use the Regional Ocean Modeling System (ROMS; available online at http://www.myroms.org), a finite difference model using terrain-following vertical coordinates, in this study. The ROMS computational kernel is described by Shchepetkin and McWilliams (1998, 2003, 2005) and Haidvogel et al. (2008). The ROMS adjoint model, which is required for the mean residence-time simulation, is well developed and has been used in numerous applications (Broquet et al. 2009; Chhak and Di Lorenzo 2007; Di Lorenzo et al. 2007; Moore et al. 2009, 2004; Powell and Moore 2009; Powell et al. 2008, 2009; Veneziani et al. 2009; Zhang et al. 2009b). The first terms in the right-hand sides of (4) and (14) were added to the ROMS code for this study. The model domain (Fig. 1) covers the NYB area. Two rivers, the Hudson and Delaware, are included. The model has 30 vertical layers and horizontal resolution of about 1 km. Chapman (1985) and Flather (1976) conditions are used for sea level elevation and barotropic velocity on the model perimeter, respectively. Tidal harmonics extracted from a regional tide simulation (Mukai et al. 2002) and remotely forced along-shelf currents deduced by Lentz (2008) are imposed on the open boundaries. An Orlanski-type radiation (Orlanski 1976) open boundary condition is used for three-dimensional momentum, temperature, and salinity, and the age and residence-time passive tracers are clamped to zero on the open boundaries. The model applies bulk formulae (Fairall et al. 2003) at the sea surface using atmospheric boundary layer conditions from the North America Regional Reanalysis (NARR; Mesinger et al. 2006). River discharge was obtained from U.S. Geological Survey (USGS) water data. A detailed description
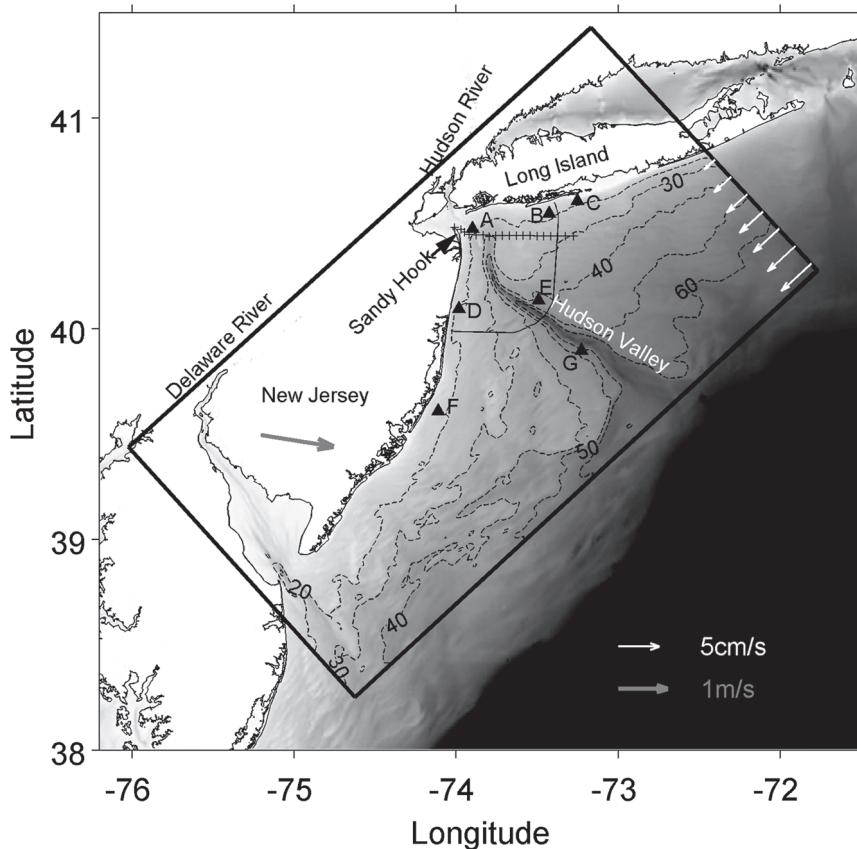
FIG. 1. The study domain: the black frame indicates the model domain; bathymetry of the NYB is in grayscale; dashed lines are contours of model isobaths in meters; gray arrow on land depicts the 2-yr (2005–06) mean wind over this area; white arrows at the northeast boundary of the model domain represent barotropic inflow boundary condition on that boundary; solid triangles are the sites for mean age and residence time referred to in the text; the line of plus symbols is the ship track on 9 Apr 2005 referred to in section 3; and the thin solid line depicts the control domain used in the residence-time simulation.

of the model configuration and verification of the model physics is given by Zhang et al. (2009a). A comparison of modeled and observed salinity along the ship track in Fig. 1 is presented in Fig. 2. The observations are from a ship-towed undulating instrument and surface CTD on 9 April 2005 (Chant et al. 2008). The model and observations show agreement in the surface salinity and vertical variation of the halocline, although the model shows a bias toward higher salinity in deep water and the low salinity anomaly that reaches 73.4°W in the observations does not extend so far eastward in the model. We note that there has been no assimilation of observations in this simulation. Model initial conditions based on a multiyear shelf-wide climatology are somewhat more salty than midshelf conditions in 2005, and we expect that this presents resistance to the spreading of the river plume and prevents low salinity water penetrating far to the east.

To simulate the mean age of Hudson River source water on the shelf, two tracers are activated in the forward ROMS model with zero initial concentration. The first is conservative and satisfies (3) with unit concentration in the Hudson River inflow, whereas the second represents the river water age concentration and satisfies (4). Its value is zero in the river inflow. Mean freshwater age is computed with (2). Regions where the concentration is lower than 10^{-5} are assumed to be free of Hudson River source water, and age there is undefined. To verify that the mean age calculation is correct, we conducted a 60-day simulation solving (1) with the full age spectrum discretized into 120 age intervals, while also computing the mean age from a concurrent simulation of C and α. The full age spectra at sites A and E in Fig. 1 at day 60 are plotted in Fig. 3; the mean age computed from the age spectra is marked, along with the corresponding mean age α/C from (2).
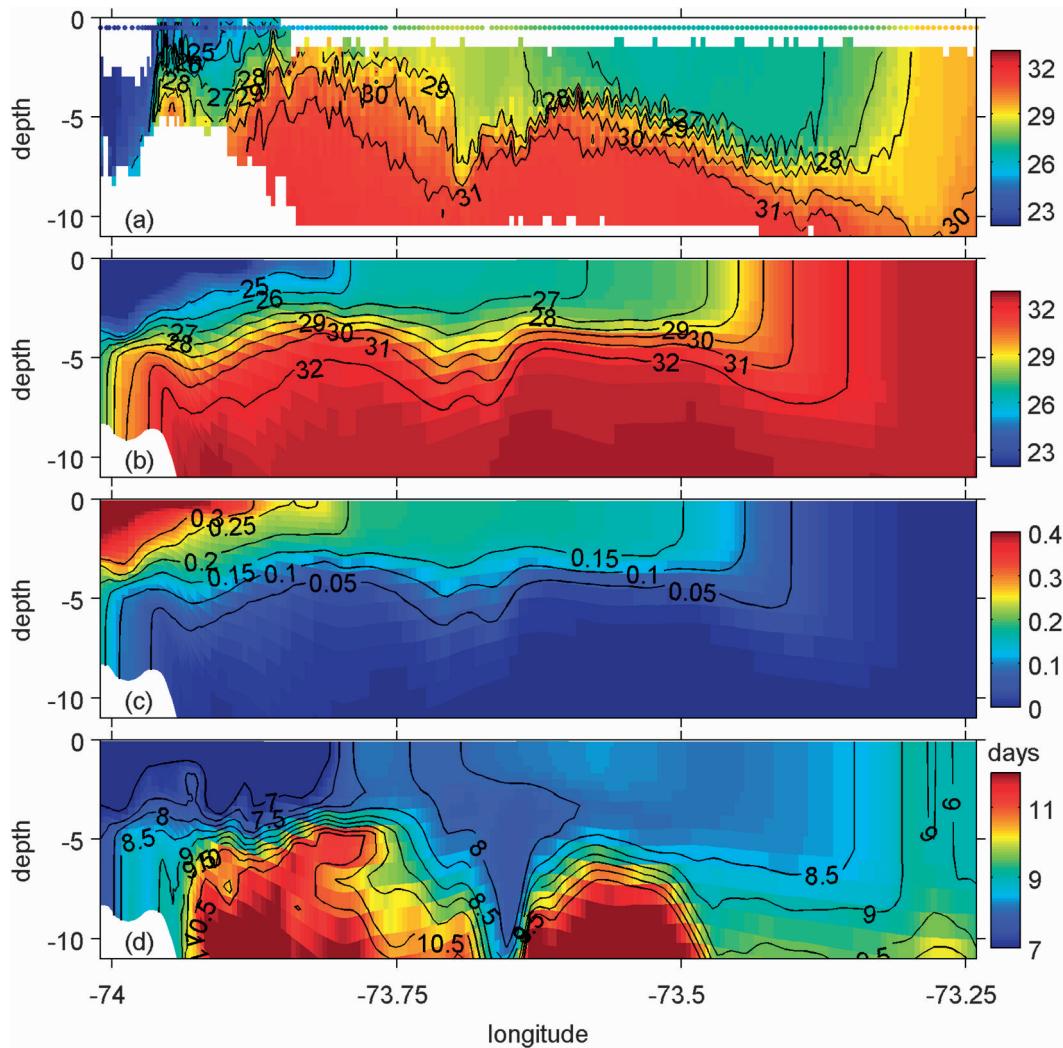
FIG. 2. Cross section of (a) observed salinity, (b) modeled salinity, (c) modeled freshwater concentration, and (d) modeled mean age along the ship track in Fig. 1.

Calculating mean age using the two-tracer approach clearly works well.

Vertical cross sections of modeled freshwater concentration and mean age are included in Fig. 2 at times corresponding to the ship-board observations. The freshwater concentration has the same pattern as modeled salinity, whereas the mean age outlines a body of relatively young (8.5 days) water around 73.4°W at the place where a similar body of freshwater was observed. This supports our claim that river water reached that location in the model, but in a smaller amount.

In the results that follow, two years of simulation (2005–06) following a spinup year (2004) form the basis of our freshwater mean age analysis. In the residence-time simulations, the control domain is defined as the surface-most 10 m of the smoothed rectangular area at

the NYB apex shown in Fig. 1. Ocean states from the three-year model simulation are stored every three hours for the background state of the adjoint model. In the adjoint model, two tracers representing the fraction of tracer remaining and the mean residence time [Eqs. (11) and (14)] are activated. The initial condition for the fraction of tracer remaining is one inside the control domain and zero everywhere outside; the mean residence time is initially zero everywhere. The adjoint model is integrated from the end of 2006 back to the beginning of 2005. No external constraints are applied to the adjoint model in the places beyond the control domain, which means residence time calculated here is the so-called exposure time. Because of tidal oscillations across the control domain perimeter, the strict residence time would misrepresent the total time that river source water spends
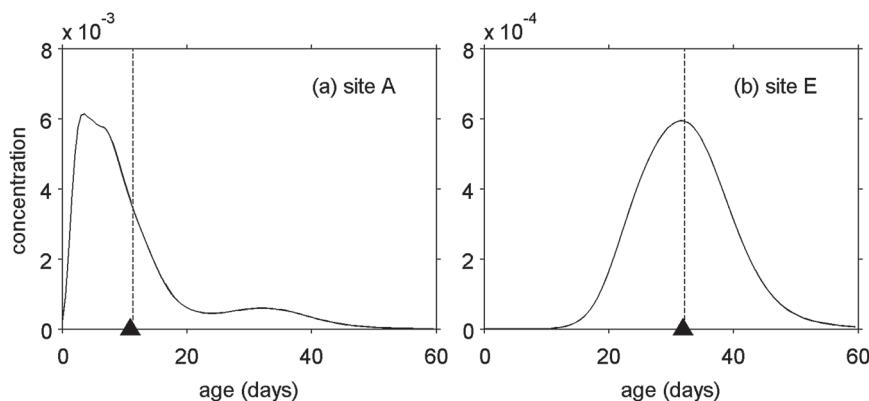
FIG. 3. Concentration distribution function (solid curves) at (a) site A and (b) site E on 10 May 2005: dashed lines indicate the mean age computed from the concentration distribution functions, and triangles indicate the mean age given by the mean age model simulation at corresponding places and time.

in the NYB area. For the sake of convenience, the term residence time is used here.

To test the validity of the adjoint-based residence-time theory and model, simulations were conducted where passive tracers injected in the forward model at selected times and locations were followed for 120 days (Fig. 4). Mean residence time computed from the fraction of each tracer remaining in the control domain is indicated by the dashed lines in Fig. 4. Comparison with the mean residence time obtained from the adjoint model (triangles in Fig. 4) shows that the two approaches generally agree. The small differences between the mean residence times could have been caused by the low resolution (half a day) in residence-time dimension or the linear interpolation used in the adjoint model simulation to obtain the nonlinear model background states between two saved snapshots.
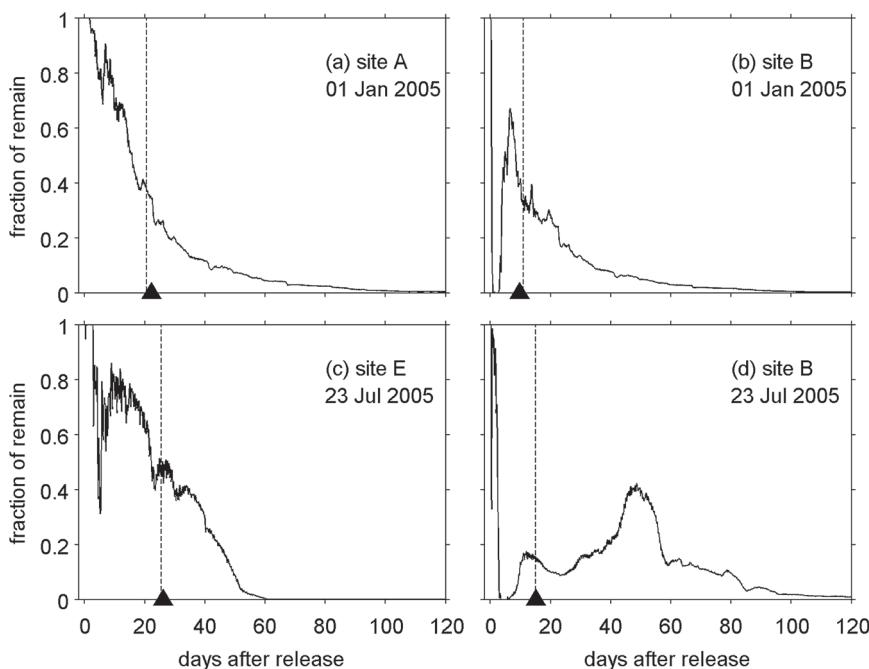
FIG. 4. Fraction of tracer remaining in the control domain after unit releases at selected sites (see Fig. 1) at different times: (a) site A 1 Jan 2005, (b) site B 01 Jan 2005, (c) site E 23 Jul 2005, and (d) site B 23 Jul 2005. Dashed lines indicate the mean residence time computed from the time series, and triangles indicate the mean residence time at the corresponding places and times given by the mean residence-time adjoint model simulation.
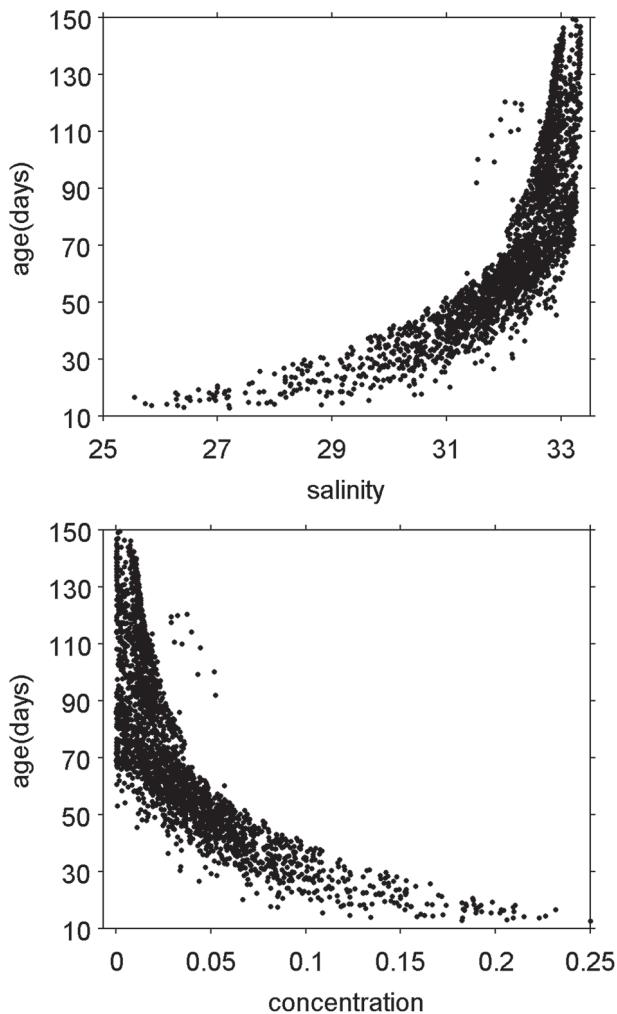
FIG. 5. Relationship between (top) salinity and (bottom) freshwater concentration and mean age at random locations in the model domain.

4. Mean age

In studies of river plume dispersal, scientists have long used salinity or concentration of a river tracer to estimate the time that river source water has been exposed in the ocean. To contrast this approach with the more rigorous mean age calculation, Fig. 5 compares mean age, salinity, and freshwater concentration at selected locations in the model. A positive relationship between mean age and salinity and inverse relationship between mean age and freshwater concentration can be seen, but by no means are the relationships linear. As the water becomes saltier and the concentration becomes lower, the range of the mean age becomes large. At salinity 33, the mean age is from 70 to 150 days. This is to be expected because the volume of river water discharged over this time scale is much smaller than that into which

it mixes; also, once the salinity becomes close to the background value of midshelf water, subsequent mixing changes the salinity little, but the water continues to age. The same logic applies to the freshwater concentration. Figure 5 suggests that estimating age from salinity or tracer concentration has limited utility and could be very misleading for time scales of more than two weeks in the case of the Hudson River plume.

a. Comparison between mean age and satellite measurements

One of our objectives in studying age and residence time is to provide estimates of the rate of physical dispersal and mixing of the river plume for future comparison to time scales of regional biogeochemical processes. We will not present here any biogeochemical process observations or results of coupled biogeochemical simulations; however, before presenting an analysis of the model results, we compare snapshots of simulated mean age with an empirical proxy for river water age derived from satellite optical observations.

Waters near the coast are turbid and optically complex (SCH). The major optical constituents of the Hudson plume are phytoplankton, sediment, colored dissolved organic matter (CDOM), and detritus, and the relative concentration and thus the optical signal of these change over time (Cahill et al. 2008; SCH). In river source plumes, CDOM is the dominant optical constituent; however, as the plume ages the CDOM signal decreases relative to phytoplankton and detrital signatures. These changes produce a spectral shift in the remote sensing reflectance (Ramadurai 2008). The ratio of reflectance at 490–670 nm wavelengths is sensitive to the relative optical signatures of CDOM and phytoplankton and therefore to the time that river source waters have been exposed in the ocean waters. This ratio, which we refer to as the 490/670 band ratio, can be computed from satellite observations by the Sea-viewing Wide Field-of-view Sensor (SeaWiFS).

Figure 6 shows many similarities in the patterns of observed 490/670 band ratio and modeled surface freshwater age during the 2005 Lagrangian Transport and Transformation Experiment (LaTTE) field experiment. We emphasize that there has been no assimilation of satellite data in these simulations; the model reproduces well the transport pathways of river water dispersal (Zhang et al. 2009a), and we expect some pattern correspondence in optical characteristics that are strongly related to the river source waters. If indeed the 490/670 band ratio is a useful proxy for water age, we further expect some correspondence in values across the four realizations in Fig. 6. To quantify the relationship, the 490/670 band ratio and mean age within the river-influenced area are plotted in Fig. 7. The correlation is 0.73, which is
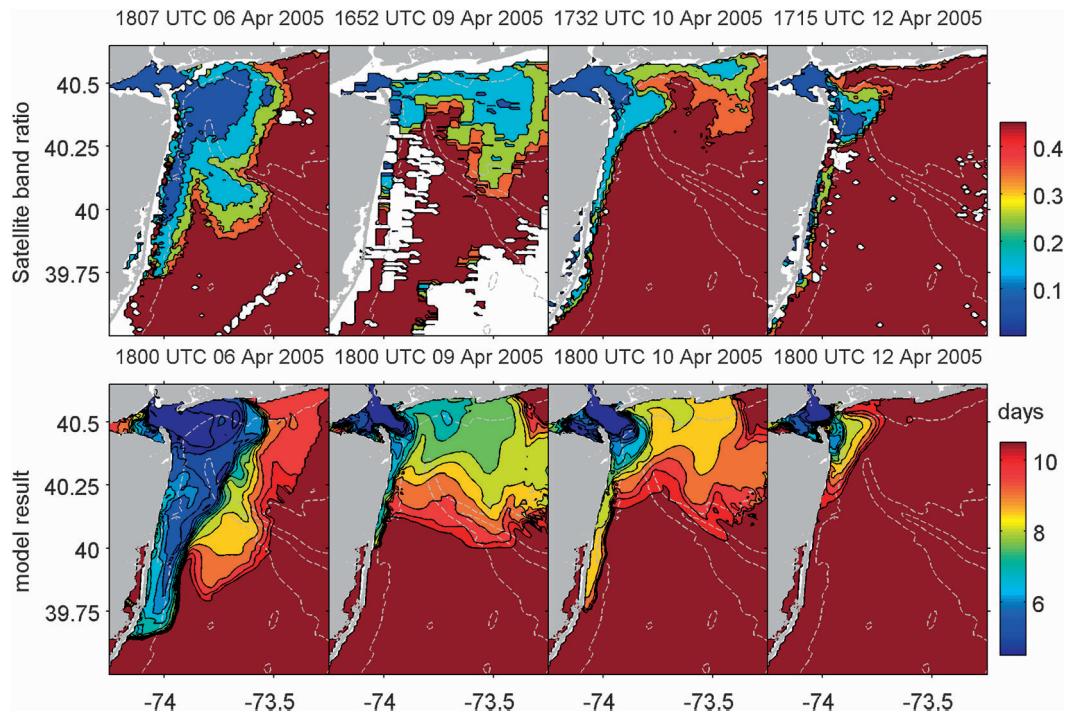
FIG. 6. Snapshots of (top) the ratio of SeaWiFS observed water leaving radiance at 490–670 nm and (bottom) modeled freshwater mean age at the sea surface. Dashed lines show 20-, 40-, and 60-m isobaths.

significant at the 95% level. A least squares fit gives $a = 1.3 + 25 \times r$, where a is the mean age and r is the band ratio. We suggest that this simple relation may have applications in field work where the age of the Hudson River–influenced waters is needed in real time. We cannot yet comment on how robust this relationship is or whether it can be employed for rivers other than the Hudson, but empirical relationships could likely be derived following the same methodology.

b. Temporal variability of the mean age

To examine temporal variability of mean age, time series of surface freshwater water concentration and mean age at sites A, C, F, and G in Fig. 1 are plotted in Fig. 8 along with river discharge and 10-day running mean filtered wind. At all the sites, the mean age fluctuates dramatically between 10 and 170 days within a few days, similar to the time scale of local wind variability. This suggests that the horizontal movement of the river plume forced by the fluctuating wind causes the variations of the mean age on short time scales. Fluctuations of mean age and freshwater concentration are inversely related. Site A, near the estuary mouth, shows the least variability, with mean age fluctuating from 10 to 40 days out of phase with the freshwater concentration and river discharge (which are closely correlated). Not surprisingly, mean age at the estuary mouth is closely related to

river discharge. Site C, near the Long Island coast, lies in the pathway along which freshwater advects eastward, principally in fall and winter (Zhang et al. 2009a). Accordingly, the mean age at site C is arguably lower in winter. Site F falls in the New Jersey coastal pathway that Zhang et al. (2009a) identified as dominating freshwater advection in winter and spring. Seasonality of this transport manifests itself in the time series of mean age: there are frequently lower age values in winter and spring and relatively high and unsteady values in summer and fall. Site G lies in the midshelf pathway that dominates the summer months and carries freshwater directly offshore (Zhang et al. 2009a); mean age at site G is generally low in summer. The mean age at site G is also low in winter 2005–06, presumably because of persistent westerlies during that time. This will be seen later in the correlation between mean age and wind.

Figure 9 presents two-year and seasonal averages of the mean age and surface current. Consistent with the three-pathway pattern of surface freshwater dispersal described by Zhang et al. (2009a), the two-year average shows farthest penetration of young water along the New Jersey coast, secondary penetration along the Long Island coast, and at about 40°N a weak offshore tongue of moderate age water along the Hudson shelf valley (HSV). The seasonal variation of mean age echoes the freshwater dispersal seasonality noted by Zhang et al.
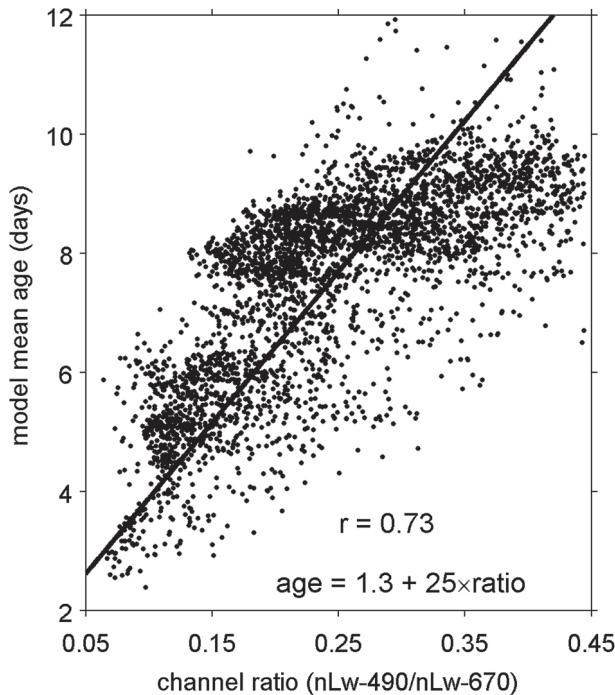
FIG. 7. Relationship between modeled mean age and the ratio of satellite-observed water leaving radiance (490–670 nm). The correlation coefficient $r = 0.73$ is significant at the 95% level. Solid line is the least squares fit: mean age = 1.3 + (25 × radiance ratio).

(2009a). In spring, relatively young water penetrates along the New Jersey coast farther than in the two-year mean and the offshore extent of moderate age water is more obvious. In summer, transport of young water along the New Jersey coast is almost completely shut down. Instead, dispersal is toward the east and the tongue of moderate age water along the HSV is pronounced, consistent with the dominance of the midshelf freshwater pathway driven by upwelling favorable wind. The pattern in fall is similar to spring, except that there is less young water along the New Jersey coast. In winter, the coastal boundary currents are stronger and young water is found considerably farther along both coasts than in the two-year mean, whereas evidence of offshore flow along the HSV is absent.

c. Relationship of mean age with river discharge and wind

In Fig. 8, mean age at site A appears correlated with the Hudson River discharge, whereas temporal variability at sites C, F, and G has time scales more akin to the wind. To quantify this, correlations of mean age with river discharge and wind are shown in Figs. 10a and 11, respectively (the wind time series used is the NARR data at 40.5°N, 73.75°W). The mean age pattern depends on the freshwater travel history, so we apply a weighted

running mean time filter to river discharge and the wind prior to the correlation analysis. This approach was used by Zhang et al. (2009a) with the filter $f_k(t) = k^{-1} \int_{-\infty}^{t} f(t') e^{(t'-t)/k} dt'$, where $f(t)$ is the wind component at time t and $f_k(t)$ is the resulting convolution with weights that decay exponentially, with scale k (Austin and Barth 2002) chosen to be characteristic of freshwater advection events in the NYB. Tests with values of k from 1 to 50 days (not shown) and time lags between wind and mean age ranging from −10 to 10 days show few differences in the correlation pattern. We use $k = 10$ days and zero lag for results in Figs. 10a and 11. For Fig. 11, note that, because we consider correlations between scalar and vector component time series, we need only show plots for wind direction in two quadrants; for example, the pattern of correlation with a strictly southerly wind is the negative of the pattern for a northerly wind.

In Fig. 10a the correlation between river discharge and mean age is negative for an area within 50 km of the New Jersey coast and as far south as Tuckerton, clearly outlining the area of direct influence of river discharge on coastal waters. Interestingly, the significant correlation extends much less far along the New York coast.

Results that are evident from Fig. 11 are that (i) easterly wind and mean age everywhere are positively correlated; (ii) as wind direction becomes increasingly southeasterly to southerly, a negative correlation emerges offshore and spreads shoreward; (iii) southerly wind is positively correlated with surface mean age on the New Jersey coast and negatively correlated with that offshore; and (iv) significant negative correlation occupies most of the coastal area when wind is westerly. The mechanism is that easterly wind pushes waters that have aged offshore back toward the coast, thereby increasing the mean age, whereas the opposite occurs for westerly winds that favor rapid dispersal of water offshore. Southerly winds cause upwelling on the New Jersey coast, which drives younger water from the coastal current eastward and lowers mean age offshore while uplifting older deep water to the surface at the coast, increasing the mean age there.

5. Mean residence time

Residence time has been used in coastal ocean studies of water renewal (Monsen et al. 2002) and biogeochemical processes (Brooks et al. 1999; Duarte et al. 2001). Residence time can be crudely estimated by dividing a total volume by a characteristic flushing rate or more accurately by releasing Lagrangian particles or Eulerian tracers into numerical models, the computational cost of which can be heavy. The capability introduced here of computing mean residence time for every location in a control domain at any time with a
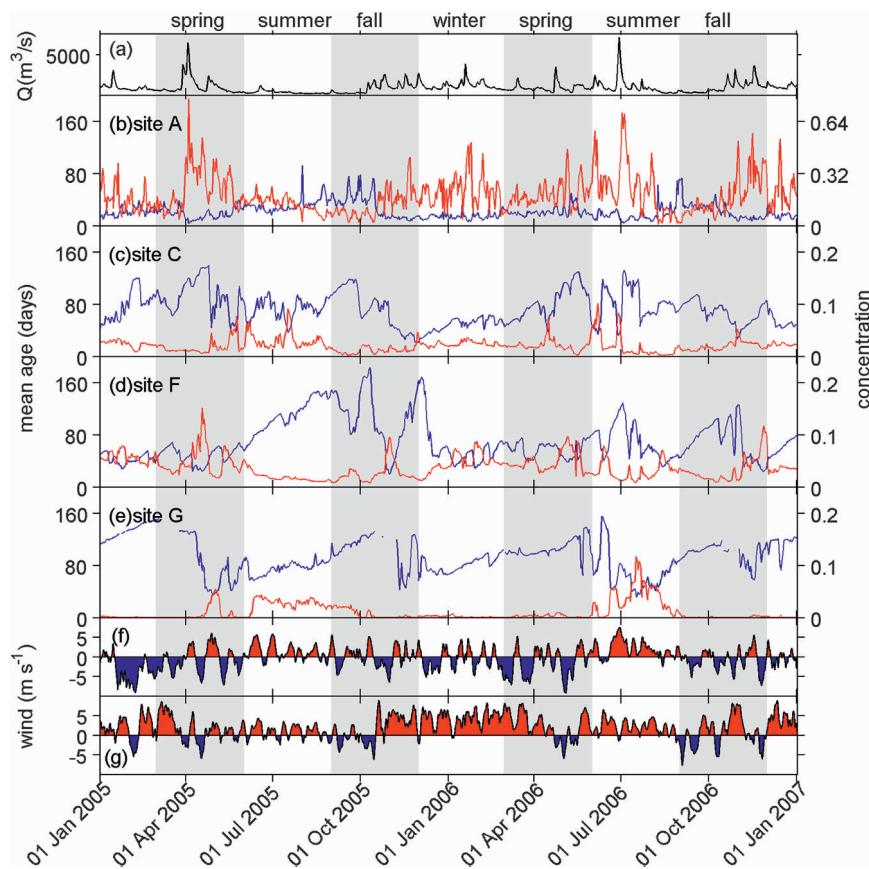
FIG. 8. Time series of (a) the Hudson River discharge and (b)–(e) freshwater concentration (red lines) and mean age (blue lines) at different sites (see Fig. 1 for locations of sites A, C, F, and G). (f) The filtered meridional (positive toward north) and (g) zonal (positive toward east) components of the wind in the NYB.

single adjoint model integration is a significant advance that provides the ability to study spatial and temporal heterogeneity of residence time and its connection with external forcing.

Because we are interested in the duration that river source water stays in the NYB, residence time in this study is defined as the numbers of days, on average, it takes water *at a particular time and location* to be flushed out of the control volume defined as the surface-most 10 m of the smoothed rectangular area shown in Fig. 1.

a. Temporal variability of mean residence time

Time series of mean residence time at four different sites in the control domain are plotted in Fig. 12 along with the fraction of tracer remaining at 1 January 2007 and wind. Recall from section 2 that, in theory, the residence-time calculation is only valid once the fraction of remaining tracer in the adjoint integration is zero, but the error becomes negligible when the fraction of remaining tracer is very small. By 1 September 2006, the tracer has vanished at all locations plotted in Fig. 12.

Accordingly, we exclude the last four months from the analysis and use only the mean residence-time values before 1 September 2006.

Before discussing these results, we restate what is being calculated in this application of the adjoint-based residence-time method: Each blue time series in Fig. 12 shows the time scale in days, after any particular date in the time series that it will subsequently take for passive tracer released at that location to be flushed out of the control volume. Residence time at site A near the harbor mouth stays around 20 days, except during summer 2005, when it often reaches 40 days. At site B, close to the eastern boundary of the control domain, residence time is generally low in winter but higher in spring and summer. The residence time at site D on the New Jersey coast does not show obvious seasonal dependence but generally varies in opposition to site B; the correlation between the time series for sites B and D is −0.36 and is significant at the 95% level. Sites B and D are located at opposite ends of the control domain, and a negative correlation is not unexpected. At site E, midshelf the
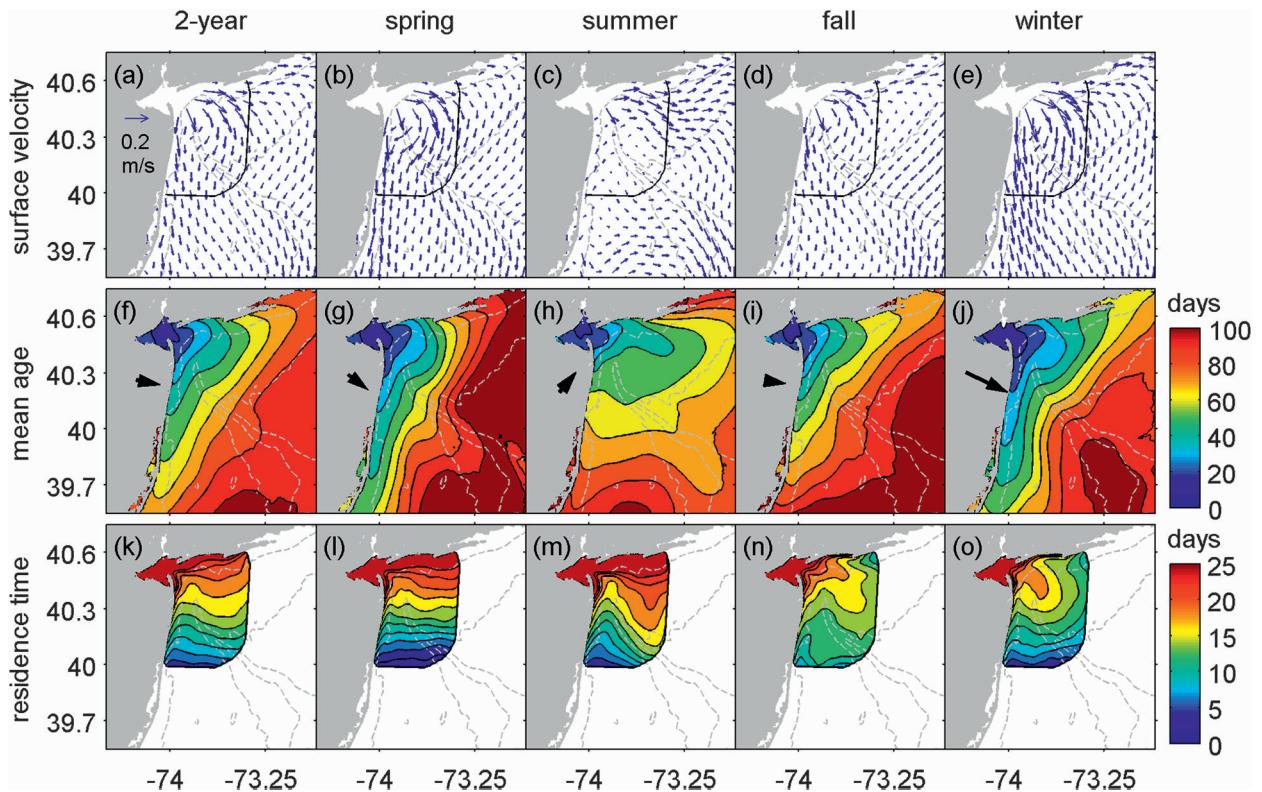
FIG. 9. Two-year mean and seasonal averages of (top) surface current, (middle) surface mean age, and (bottom) surface residence time. (middle) Black arrows indicate direction and relative strength of the average wind stress. Dashed lines show the 20-, 40-, and 60-m isobaths.

residence time is generally lower than 20 days, except during summer 2005. The correlation between residence times at site D and B is 0.27, which is significant (95% level). These sites are both located north of the HSV, which Zhang et al. (2009a) showed places them in a related circulation regime, and the similarity in residence-time variability is therefore reasonable. The residence times at sites A, B, and E all exhibit generally high values in summer, which is clear in the seasonal average residence time in Fig. 9 (bottom row).

The two-year average residence time shown in Fig. 9 has highest values in the estuary and along the Long Island coast and lower values south of the HSV, and these features are shared by all the seasonal averages, although differences between the seasonal averages exist. Mean residence time along the Long Island coast in spring and summer is much higher than in fall and winter, which is consistent with the sense we obtained from the time series (Fig. 12). In summer, the HSV clearly serves as a barrier between zones of relatively high residence time to the north and low residence time to the south. The influence of the HSV in other seasons is not as obvious. In winter, a circular feature of high residence time occurs in the New York Bight apex area that is

similar to the river water bulge in Zhang et al. (2009a), indicating that in winter the recirculating bulge traps water and prolongs its residence in the NYB apex.

Residence time is very large along the Long Island coast in summer, all the way to the eastern edge of the control volume, despite there being a strong eastward surface current that transports water swiftly along the Long Island coast, enabling it to quickly exit the control domain. The mechanism behind this apparent paradox is revealed by the concentration of a passive tracer released at site B during summer 2005; the time series of the fraction of tracer remaining in the control domain is plotted in Fig. 4d. There is indeed a rapid decline of tracer right after release, but as time proceeds a substantial fraction of the tracer returns: some 40% of the initial release at site B reenters the control domain 50 days later. What has occurred is that eastward flow along the Long Island coast in summer has carried the tracer out of the control domain, but the tracer has remained nearby on the inner shelf and the change to southwestward flow in the fall has pushed the tracer back into the control domain, from which it subsequently exits through the southern boundary. Flow across the eastern boundary of the control domain is only a temporary outlet for
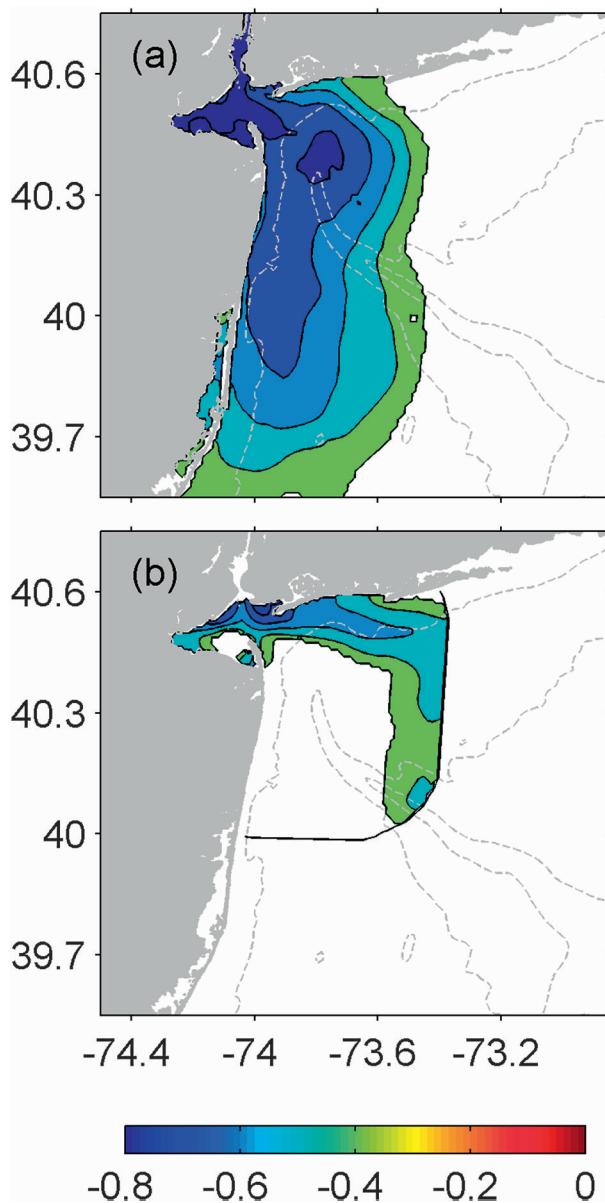
FIG. 10. Correlation between (a) surface mean age and (b) surface mean residence time and 10-day time-scale running mean low-pass filtered Hudson River discharge. Only correlations significant at the 95% level and greater than 0.3 are plotted. Contours are in 0.1 intervals. Dashed lines show the 20-, 40-, and 60-m isobaths.

tracers in the NYB apex; transport across the southern boundary is the real exit.

This reentry process is given full consideration in the adjoint-based residence-time method, because we compute the accumulated tracer exposure time as explained in section 3. This is potentially very important when employing residence-time estimates in studies of, for example, river-borne pollutant dispersal, degradation and bioaccumulation, phytoplankton growth and secondary productivity, or larval transport and settlement. All of these are influenced by processes active on time scales of a few to several tens of days, and the strict mean residence time as opposed to exposure time could represent time scales significantly differently.

b. Relationship of mean residence time with river discharge and wind

In a similar manner to mean age, mean residence time fluctuates dramatically on short time scales, presumably because of wind-driven movement of the river plume. To quantify the relationships, we computed correlations of residence time with the Hudson River discharge and the wind as shown in Figs. 10b and 13, respectively. Because the dispersal of water over the finite expanse of the control region relies on the accumulated effect of buoyancy- and wind-driven flow over some time, the river discharge and wind components were weighted using a running mean filter, $f_k(t) = k^{-1} \int_t^{+\infty} f(t') e^{(t-t')/k} \, dt'$, similar to that used in section 4c. Note that the filter acts on times strictly after the release time, because it is river discharge and wind in the future subsequently influences the dispersal and residence time of the tracer. Different filter scales k and time lags were tested but again few differences occur in the correlation patterns (not shown). A 10-day filter time scale and zero lag are used in the results in Figs. 10b and 13.

Figure 10b shows that significant correlation between river discharge and residence time occurs only along the Long Island coast and eastern boundary of the control domain and is negative; that is, high river discharge decreases residence time for waters starting from a those locations. This pattern of negative correlation echoes the outer boundary of the circular freshwater pathway in the NYB shown by Zhang et al. (2009a). It presumably occurs because high river discharge accelerates the bulge and sweeps water at the outer extent of the recirculation from the control domain.

Figure 13 shows that easterly wind is positively correlated with residence time near the Long Island coast but negatively correlated with residence time between the New Jersey coast and HSV. We have already seen that easterly winds drive westward flow along the Long Island coast that prolong residence time there, whereas westerly winds flush Long Island coastal waters and lower residence time. However, easterly wind also pushes to the west surface waters that lie between the New Jersey coast and the HSV, strengthening the New Jersey coastal current (Choi and Wilkin 2007) and lowering the time waters from this region stay in the control domain. When winds are more southeasterly, the pattern of negative correlation between New Jersey and the HSV disappears. A positive correlation between residence time and winds
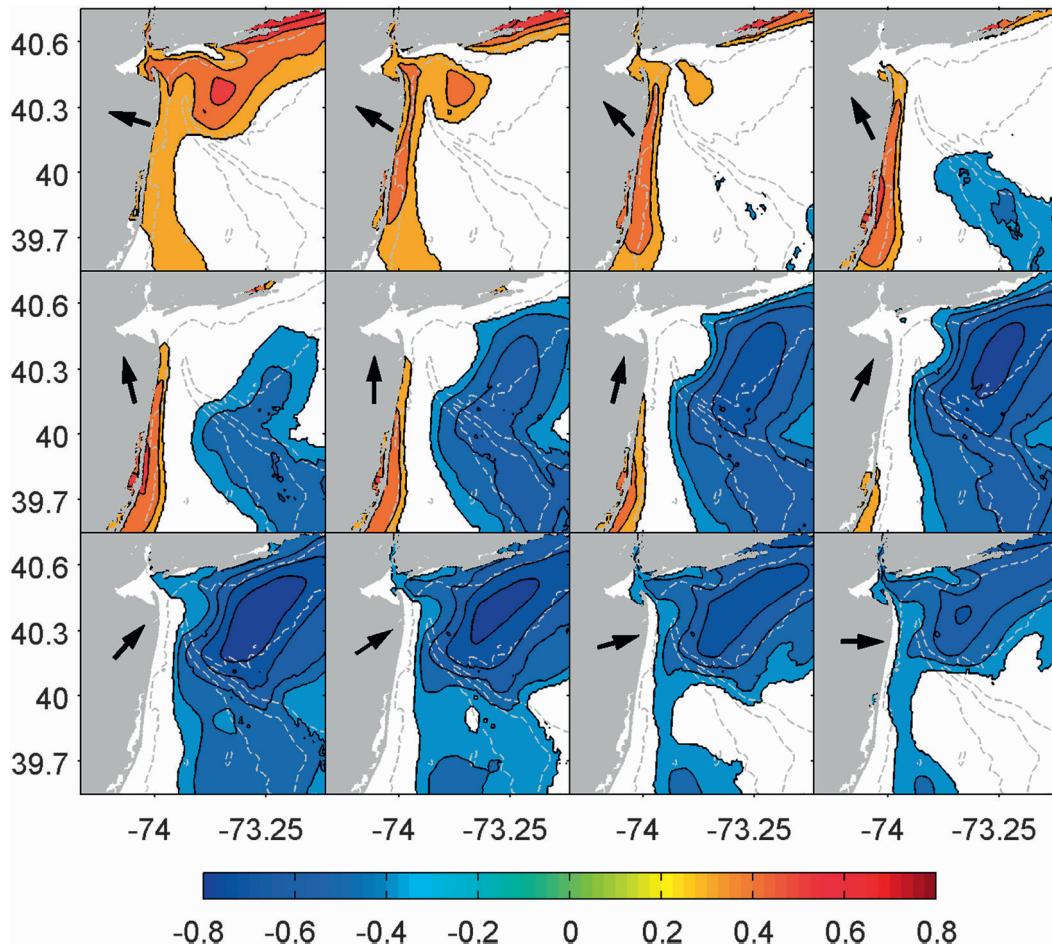
FIG. 11. Correlation between surface mean age and 10-day time-scale running mean low-pass-filtered wind components in different direction. Arrows on land depict the wind direction. Only correlations significant at the 95% level and >0.3 are plotted. Contour interval is 0.1. Dashed lines show the 20-, 40-, and 60-m isobaths.

from the south and west occurs along the New Jersey coast and inner shelf because either upwelling (southwesterly wind) directs surface water northward and eastward, extending the time water next to the New Jersey coast stays in the control domain, or downwelling (northeasterly wind) pushes surface water into the coastal current, which promptly exits the control domain, or both.

6. Summary and discussion

This study extends modeling studies by Zhang et al. (2009a) and Choi and Wilkin (2007) to consider in detail the time scales associated with dispersal of Hudson River source water within the New York Bight. We have restated constituent-oriented age and residence-time theory and summarized application of the theory in ROMS, including verification that two-tracer-based mean age and adjoint-based residence-time methods give the same results as more conventional multitracer methods.

The mean age results here should be interpreted as the mean time since water at a given location and time entered into the ocean via the Hudson River. The mean recognizes that a water mass at any location comprises some younger water that has traveled relatively rapidly to the site mixed with older waters that have taken a less direct route. Detailed information about the full age spectrum of water at a particular location and time is not considered in this study because of the large computational effort required. Rather, we focus on the first moment of the age distribution (i.e., the mean age) given by an inexpensive two-tracer simulation. This is of value when the objective is explicit consideration of average dispersal and dilution time scales.

The model results show a linear relationship, though noisy, between modeled surface mean age and the ratio of satellite-measured radiances at 490 and 670 nm, which has been proposed as an empirical proxy of age. A least squares fit of age on band ratio is a potentially useful tool
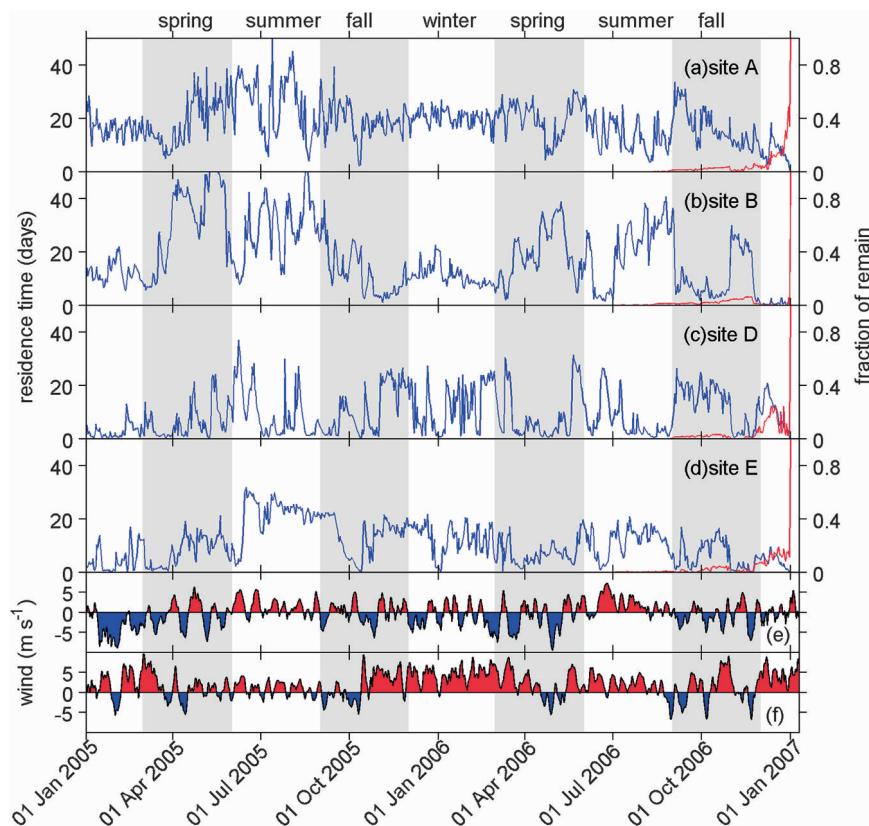
FIG. 12. (a)–(d) Time series at different sites of mean residence time (blue lines) and fraction of tracer remaining in the control domain (red lines) (see Fig. 1 for site locations) and 10-day running mean filtered wind components in the (e) meridional and (f) zonal directions.

for estimating water age from remotely sensed observations, though analysis of a more extensive dataset is required to formulate a robust relationship. Time series of mean age at different sites in the NYB show significant temporal and spatial variation in mean age, indicating that the tracer field is being stirred but has not yet been homogenized by mixing processes. Within 50 km of the New Jersey coast, mean age is strongly influenced by the river discharge, but no such influence is obvious for the area beyond. Rather, temporal variability of mean age on the scale of days is consistent with a dominant influence from wind, and this carries through to seasonal differences in mean age patterns related to seasonality in prevailing wind.

What we gain in this age analysis over conventional simulations of mean velocity and salinity is explicit information on time scales. Figure 9 shows that, in the long-term average, Hudson River–influenced waters take 60 days to reach the Long-term Ecosystem Observatory-15 (LEO-15) site on the Jersey Shore (near site F in Fig. 1). Most ecosystem and geochemical processes that would act on river-borne material could reasonably be expected to be mature by this time, suggesting it is unlikely there

is much direct influence of the Hudson on the coastal ocean this far south. The mean age at LEO-15 almost halves to roughly 35 days in winter and spring, allowing the likelihood of a significantly greater impact from the river during those seasons. The time series for site F in Fig. 8d shows that, at LEO-15, the mean age can plunge dramatically from highs far exceeding 100 days to low values less than 30 days in the course of a few weeks or less, seemingly with the onset of northwesterly winds (Fig. 11). Such rapid changes indicate that patches of rather different mean age water exist on the inner shelf and therefore that, close to shore and well south of New York Harbor, the waters originating from the Hudson River are still not laterally well mixed.

The adjoint model residence-time analysis is based on slightly less than two years of simulation. Here, we defined a control volume encompassing most of the NYB within 50 km of the mouth of the Hudson estuary. Our interpretation of residence time is the number of days it takes for a tracer to be flushed out of this control volume and not return. The results are dependent not only on starting location (i.e., proximity to the edge of the control domain) but also time because of variation in the
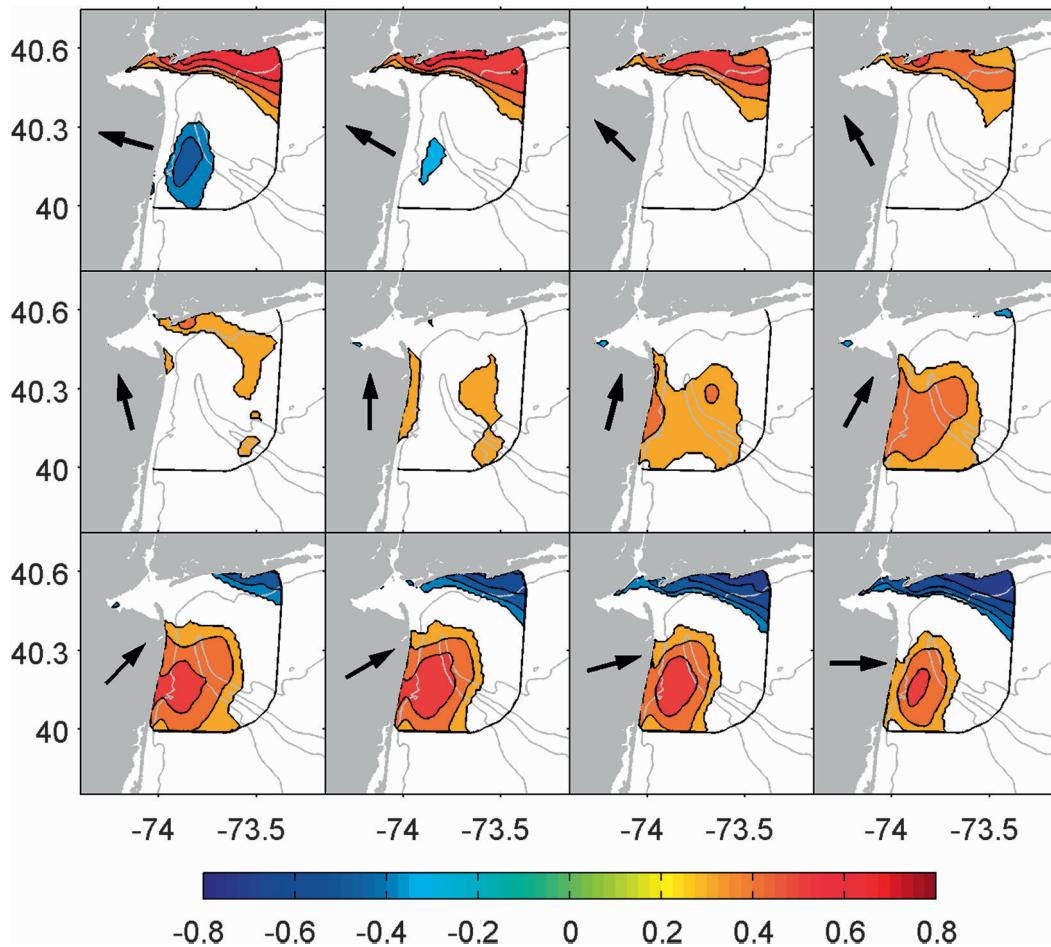
FIG. 13. Correlation between surface mean residence time and filtered wind components in different directions. Arrows on land depict the wind direction. Only correlations significant at the 95% level and >0.3 are plotted. Contour interval is 0.1. Gray lines show the 20-, 40-, and 60-m isobaths.

transport pathways by which tracer is exported from the control domain.

As was the case for age and passive tracers, the mean residence time exhibits strong temporal fluctuations on the scale of days in response to river discharge and wind, and seasonal averages show some differences in spatial pattern. In all seasons, residence time is long near to the estuary mouth and along the Long Island coast and short along the southern boundary of the control domain. High values along the Long Island coast where a strong but variable eastward boundary current forms were somewhat unexpected, and the mechanism behind this is that water that previously exited the control domain in spring and summer reenters when winds change to easterly. The recirculating low salinity bulge at the estuary mouth that forms during high river discharge events and is a conspicuous feature of winter circulation is a trap that extends residence times by 5–10 days compared to waters outside the bulge.

The Hudson River is the major source of nutrient and contaminants for the NYB, and the apex region has historically been the site of significant dumping of urban waste. Age and residence time together provide complementary information about the extent to which biogeochemical processes might act on human impacted waters as they move through this region. The time it takes river injected tracers to reach places on the shelf is a key factor in estimating the uptake rate of nutrients by phytoplankton (SCH) and to measure enzyme activities (Gaas 2010), to give two examples for this region. Age information can therefore assist the selection of rate parameters in simulating biogeochemical processes, which is one of the main difficulties in ecosystem modeling. The time it takes tracers to flush out of the NYB apex area is relevant to studies of larval or contaminant dispersal. The survival rate of some larvae depends heavily on the time they can stay in certain water conditions or a specific area (Cowen 2002; Steves et al. 1999). The spatial and temporal

variability of residence time demonstrated here suggests that spawning time and location could be a critical factor influencing survival. The residence-time information can therefore potentially be used in the study of ecological population dynamics. For ocean contamination prevention and containment, the mean age simulation gives the average travel time from a continuous contamination source to a specific location in the ocean; complementarily, the mean residence-time simulation gives the exposure of a defined area to instantaneously released pollution.

We have demonstrated here that temporally and spatially resolved information on these time scales can be computed in a coastal ocean model using mean age calculated from just two model tracers (conservative and age concentration) and residence time provided by a single integration of an adjoint model. Together, they provide a rather complete coverage of the time scales in a specific ocean area. The formulation of control domains and age tracer release scenarios are readily adapted to address questions of specific relevance to other applications.

REFERENCES

Adams, D. A., J. S. O'Connor, and S. B. Weisberg, 1998: Sediment quality of the NY/NJ harbor system. EPA Final Rep. EPA/902-R-98-001, 126 pp.

Austin, J. A., and J. A. Barth, 2002: Variation in the position of the upwelling front on the Oregon shelf. *J. Geophys. Res.,* **107,** 3180, doi:10.1029/2001JC000858.

Brooks, D. A., M. W. Baca, and Y.-T. Lo, 1999: Tidal circulation and residence time in a macrotidal estuary: Cobscook Bay, Maine. *Estuarine Coastal Shelf Sci.,* **49,** 647–665.

Broquet, G., C. A. Edwards, A. M. Moore, B. S. Powell, M. Veneziani, and J. D. Doyle, 2009: Application of 4D-Variational data assimilation to the California Current System. *Dyn. Atmos. Oceans,* **48,** 69–92, doi:10.1016/j.dynatmoce.2009.03.001.

Cahill, B., O. Schofield, R. Chant, J. Wilkin, E. Hunter, S. Glenn, and P. Bissett, 2008: Dynamics of turbid buoyant plumes and the feedbacks on near-shore biogeochemistry and physics. *Geophys. Res. Lett.,* **35,** L10605, doi:10.1029/2008GL033595.

Castelao, R., O. Schofield, S. Glenn, R. Chant, and J. Kohut, 2008: Cross-shelf transport of fresh water on the New Jersey shelf. *J. Geophys. Res.,* **113,** C07017, doi:10.1029/2007JC004241.

Chant, R. J., S. M. Glenn, E. Hunter, J. Kohut, R. F. Chen, R. W. Houghton, J. Bosch, and O. Schofield, 2008: Bulge formation of a buoyant river flow. *J. Geophys. Res.,* **113,** C01017, doi:10.1029/2007JC004100.

Chapman, D. C., 1985: Numerical treatment of cross-shelf open boundaries in a barotropic ocean model. *J. Phys. Oceanogr.,* **15,** 1060–1075.

Chhak, K., and E. Di Lorenzo, 2007: Decadal variations in the California Current upwelling cells. *Geophys. Res. Lett.,* **34,** L14604, doi:10.1029/2007GL030203.

Choi, B.-J., and J. L. Wilkin, 2007: The effect of wind on the dispersal of the Hudson River plume. *J. Phys. Oceanogr.,* **37,** 1878–1897.

Cowen, R. K., 2002: Oceanographic influences on larval dispersal and retention and their consequences for population connectivity. *Coral Reef Fishes: Dynamics and Diversity in a Complex Ecosystem,* P. F. Sale, Ed., Academic Press, 149–170.

Deleersnijder, E., J.-M. Campin, and E. J. M. Delhez, 2001: The concept of age in marine modelling: I. Theory and preliminary model results. *J. Mar. Syst.,* **28,** 229–267.

Delhez, E. J. M., 2006: Transient residence and exposure time. *Ocean Sci.,* **2,** 1–9.

——, and E. Deleersnijder, 2006: The boundary layer of the residence time field. *Ocean Dyn.,* **56,** 139–150, doi:10.1007/s10236-006-0067-0.

——, J.-M. Campin, A. C. Hirst, and E. Deleersnijder, 1999: Toward a general theory of the age in ocean modeling. *Ocean Modell.,* **1,** 17–27.

——, E. Deleersnijder, A. Mouchet, and J.-M. Beckers, 2003: A note on the age of radioactive tracers. *J. Mar. Syst.,* **38,** 277–286.

——, A. W. Heemink, and E. Deleersnijder, 2004: Residence time in a semi-enclosed domain from the solution of an adjoint problem. *Estuarine Coastal Shelf Sci.,* **61,** 691–702.

Di Lorenzo, E., A. M. Moore, H. G. Arango, B. D. Cornuelle, A. J. Miller, B. Powell, B. S. Chua, and A. Bennett, 2007: Weak and strong constraint data assimilation in the inverse Regional Ocean Modeling System (ROMS): Development and application for a baroclinic coastal upwelling system. *Ocean Modell.,* **16,** 160–187.

Duarte, A. S., J. L. Pinho, M. A. Pardal, J. M. Neto, J. P. Vieira, and F. S. Santos, 2001: Effect of residence times on River Mondego estuary eutrophication vulnerability. *Water Sci. Technol.,* **44,** 329–336.

England, M. H., 1995: The age of water and ventilation timescales in a global ocean model. *J. Phys. Oceanogr.,* **25,** 2756–2777.

Fairall, C. W., E. F. Bradley, J. E. Hare, A. A. Grachev, and J. Edson, 2003: Bulk parameterization of air–sea fluxes: Updates and verification for the COARE algorithm. *J. Climate,* **16,** 571–591.

Fine, R. A., 1995: Tracers, timescales, and the thermohaline circulation: the lower limb in the North Atlantic Ocean. *Rev. Geophys.,* **33** (Suppl.), 1353–1365.

Flather, R. A., 1976: A tidal model of the northwest European continental shelf. *Mem. Soc. Roy. Sci. Liege.,* **6,** 141–164.

Gaas, B., 2010: Response and regulation of cell-surface hydrolases to nutrient stress in river-influenced coastal areas. Ph.D. dissertation, Rutgers University Institute of Marine and Coastal Sciences, 120 pp.

Gao, Y., H. Drange, M. Bentsen, and O. M. Johannessen, 2005: Tracer-derived transit time of the waters in the eastern Nordic Seas. *Tellus,* **57B,** 332–340.

Garvine, R. W., 2004: The vertical structure and subtidal dynamics of the inner shelf off New Jersey. *J. Mar. Res.,* **62,** 337–371, doi:10.1357/0022240041446182.

Geyer, W. R., J. D. Woodruff, and P. Traykovski, 2001: Sediment transport and trapping in the Hudson River estuary. *Estuaries,* **24,** 670–679.

Haidvogel, D. B., and Coauthors, 2008: Ocean forecasting in terrain-following coordinates: Formulation and skill assessment of the Regional Ocean Modeling System. *J. Comput. Phys.,* **227,** 3595–3624.

Haine, T. W. N., and T. M. Hall, 2002: A generalized transport theory: Water-mass composition and age. *J. Phys. Oceanogr.,* **32,** 1932–1946.

——, A. J. Watson, M. I. Liddicoat, and R. R. Dickson, 1998: The flow of Antarctic bottom water to the southwest Indian Ocean estimated using CFCs. *J. Geophys. Res.,* **103,** 27 637–27 653.

Hall, T. M., and R. A. Plumb, 1994: Age as a diagnostic of stratospheric transport. *J. Geophys. Res.,* **99,** 1059–1070.

——, and T. W. N. Haine, 2002: On ocean transport diagnostics: The idealized age tracer and the age spectrum. *J. Phys. Oceanogr.,* **32,** 1987–1991.

Hohmann, R., M. Hofer, R. Kipfer, F. Peeters, D. M. Imboden, H. Baur, and M. N. Shimaraev, 1998: Distribution of helium and tritium in Lake Baikal. *J. Geophys. Res.,* **103,** 12 823–12 838.

Holzer, M., and T. M. Hall, 2000: Transit-time and tracer-age distributions in geophysical flows. *J. Atmos. Sci.,* **57,** 3539–3558.

Howarth, R. W., R. Marino, D. P. Swaney, and E. W. Boyer, 2006: Wastewater and watershed influences on primary productivity and oxygen dynamics in the lower Hudson River estuary. *The Hudson River Estuary,* J. S. Levington and J. R. Waldman, Eds., Cambridge University Press, 121–139.

Jenkins, W. J., 1987: ^{3}H and ^{3}He in the beta triangle: Observations of gyre ventilation and oxygen utilization rates. *J. Phys. Oceanogr.,* **17,** 763–783.

Johnson, D. R., J. Miller, and O. Schofield, 2003: Dynamics and optics of the Hudson River outflow plume. *J. Geophys. Res.,* **108,** 3323, doi:10.1029/2002JC001485.

Khatiwala, S., 2007: A computational framework for simulation of biogeochemical tracers in the ocean. *Global Biogeochem. Cycles,* **21,** GB3001, doi:10.1029/2007GB002923.

Lanczos, C., 1961: *Linear Differential Operators.* D. Van Nostrand, 580 pp.

Lentz, S. J., 2008: Observations and a model of the mean circulation over the Middle Atlantic Bight continental shelf. *J. Phys. Oceanogr.,* **38,** 1203–1221.

Malone, T. C., and M. B. Chervin, 1979: The production and fate of phytoplankton size fractions in the plume of the Hudson River, New York Bight. *Limnol. Oceanogr.,* **24,** 683–696.

Mesinger, F., and Coauthors, 2006: North American Regional Reanalysis. *Bull. Amer. Meteor. Soc.,* **87,** 343–360.

Moline, M. A., and Coauthors, 2008: Biological responses in a dynamic, buoyant river plume. *Oceanography,* **21,** 70–89.

Monsen, N. E., J. E. Cloern, L. V. Lucas, and S. G. Monismith, 2002: A comment on the use of flushing time, residence time, and age as transport time scales. *Limnol. Oceanogr.,* **47,** 1545–1553.

Moore, A. M., H. G. Arango, E. Di Lorenzo, B. D. Cornuelle, A. J. Miller, and D. J. Neilson, 2004: A comprehensive ocean prediction and analysis system based on the tangent linear and adjoint of a regional ocean model. *Ocean Modell.,* **7,** 227–258.

——, ——, ——, A. J. Miller, and B. D. Cornuelle, 2009: An adjoint sensitivity analysis of the Southern California Current circulation and ecosystem. Part I: The physical circulation. *J. Phys. Oceanogr.,* **39,** 702–720.

Mukai, A. Y., J. J. Westerink, R. A. Luettich Jr., and D. Mark, 2002: Eastcoast 2001, a tidal constituent database for the western North Atlantic, Gulf of Mexico, and Caribbean Sea. ERDC/CHL Tech. Rep. TR-02-24, 196 pp.

Orlanski, I., 1976: A simple boundary condition for unbounded hyperbolic flows. *J. Comput. Phys.,* **21,** 251–269.

Powell, B. S., and A. M. Moore, 2009: Estimating the 4DVAR analysis error of GODAE products. *Ocean Dyn.,* **59,** 121–138, doi:10.1007/s10236-008-0172-3.

——, H. G. Arango, A. M. Moore, E. Di Lorenzo, R. F. Milliff, and D. Foley, 2008: 4DVAR data assimilation in the Intra-Americas Sea with the Regional Ocean Modeling System (ROMS). *Ocean Modell.,* **25,** 173–188, doi:10.1016/j.ocemod.2008.08.002.

——, A. M. Moore, H. Arango, E. Di Lorenzo, R. Milliff, and R. R. Leben, 2009: Near real-time assimilation and prediction in the Intra-Americas Sea with ROMS. *Dyn. Atmos. Oceans,* **48,** 46–68.

Ramadurai, R., 2008: Water mass classification using band ratios. M.S. thesis, Rutgers University Institute of Marine and Coastal Sciences, 101 pp.

Sarmiento, J. L., G. Thiele, R. M. Key, and W. S. Moore, 1990: Oxygen and nitrate new production and remineralization in the North Atlantic subtropical gyre. *J. Geophys. Res.,* **95,** 18 303–18 315.

Schlosser, P., J. L. Bullister, R. A. Fine, W. J. Jenkins, R. Key, J. Lupton, W. Roether, and W. M. Smethie Jr., 2001: Transformation and age of water masses. *Ocean Circulation and Climate,* G. Siedler, J. Church, and J. Gould, Eds., Academic Press, 431–454.

Shchepetkin, A. F., and J. C. McWilliams, 1998: Quasi-monotone advection schemes based on explicit locally adaptive diffusion. *Mon. Wea. Rev.,* **126,** 1541–1580.

——, and ——, 2003: A method for computing horizontal pressure-gradient force in an oceanic model with a nonaligned vertical coordinate. *J. Geophys. Res.,* **108,** 3090, doi:10.1029/2001JC001047.

——, and ——, 2005: The Regional Oceanic Modeling System (ROMS): A split-explicit, free-surface, topography-following-coordinate oceanic model. *Ocean Modell.,* **9,** 347–404.

Steves, B. P., R. K. Cowen, and M. H. Malchoff, 1999: Settlement and sursery habitants for demersal fishes on the continental shelf of the New York Bight. *Fish. Bull.,* **98,** 167–188.

Thiele, G., and J. L. Sarmiento, 1990: Tracer dating and ocean ventilation. *J. Geophys. Res.,* **95,** 9377–9391.

Veneziani, M., C. A. Edwards, and A. M. Moore, 2009: A central California coastal ocean modeling study: 2. Adjoint sensitivities to local and remote driving mechanisms. *J. Geophys. Res.,* **114,** C04020, doi:10.1029/2008JC004775.

Waugh, D. W., T. M. Hall, and T. W. N. Haine, 2003: Relationships among tracer ages. *J. Geophys. Res.,* **108,** 3138, doi:10.1029/2002JC001325.

Weiss, R. F., E. C. Carmack, and V. M. Koropalov, 1991: Deep-water renewal and biological production in Lake Baikal. *Nature,* **349,** 665–669, doi:10.1038/349665a0.

Wong, K.-C., 1999: The wind driven currents on the Middle Atlantic Bight inner shelf. *Cont. Shelf Res.,* **19,** 757–773, doi:10.1016/S0278-4343(98)00107-1.

Wunsch, C., 2002: Oceanic age and transient tracers: Analytical and numerical solutions. *J. Geophys. Res.,* **107,** 3048, doi:10.1029/2001JC000797.

Yankovsky, A. E., R. W. Garvine, and A. Munchow, 2000: Mesoscale currents on the inner New Jersey shelf driven by the interaction of buoyancy and wind forcing. *J. Phys. Oceanogr.,* **30,** 2214–2230.

Zhang, W. G., J. L. Wilkin, and R. J. Chant, 2009a: Modeling the pathways and mean dynamics of river plume dispersal in New York Bight. *J. Phys. Oceanogr.,* **39,** 1167–1183.

——, ——, J. C. Levin, and H. G. Arango, 2009b: An adjoint sensitivity study of buoyancy- and wind-driven circulation on the New Jersey inner shelf. *J. Phys. Oceanogr.,* **39,** 1652–1668.